Proc. Natl. Acad. Sci. USA
Vol. 96, pp. 2776–2781, March 1999
Biophysics

Interpretation of the spatial charge displacements in bacteriorhodopsin in terms of structural changes during the photocycle

ANDRÁS DÉR*†‡, LÁSZLÓ OROSZI*, ÁGNES KULCSÁR*, LÁSZLÓ ZIMÁNYI*, RUDOLF TÓTH-BOCONÁDI*†, LAJOS KESZTHELYI*, WALTHER STOECKENIUS§, AND PÁL ORMOS*

*Institute of Biophysics, Biological Research Center of the Hungarian Academy of Sciences, P.O. Box 521, Szeged H-6701, Hungary; †Grenoble High Magnetic Field Laboratory, 25 Avenue des Martyrs, BP 166, 38042 Grenoble Cedex 9, France; and §Department of Chemistry, University of California Santa Cruz, Santa Cruz, CA, 95064

Contributed by Walther Stoeckenius, January 4, 1999

ABSTRACT **We have recently introduced a method, made possible by an improved orienting technique using a combination of electric and magnetic fields, that allows the three-dimensional detection of the intramolecular charge displacements during the photocycle of bacteriorhodopsin. This method generates electric asymmetry, a prerequisite for the detection of electric signal on the macroscopic sample, in all three spatial dimensions. Purple membrane fragments containing bacteriorhodopsin were oriented so that their permanent electric dipole moment vectors were perpendicular to the membrane plane and pointed in the same direction. The resulting cylindrical symmetry was broken by photoselection, *i. e.*, by flash excitation with low intensity linearly polarized light. From the measured electric signals, the three-dimensional motion of the electric charge center in the bacteriorhodopsin molecules was calculated for the first 400 μs. Simultaneous absorption kinetic recording provided the time-dependent concentrations of the intermediates. Combining the two sets of data, we determined the discrete dipole moments of intermediates up to M. When compared with the results of current molecular dynamics calculations, the data provided a decisive experimental test for selecting the optimal theoretical model for the proton transport and should eventually lead to a full description of the mechanism of the bacteriorhodopsin proton pump.**

Bacteriorhodopsin (bR) is an integral protein in the plasma membrane of *Halobacterium salinarum* (1). Upon light absorption, bR transports protons across the membrane, converting the photon energy into the energy of a proton electrochemical gradient (for recent reviews, see refs. 2 and 3). bR is a single small protein and is the simplest known active ion pump and biological light energy transducer. Consequently, it is a prototype system for studying the basic steps and rules of biological energy transduction. bR consists of the 23-kDa protein moiety and a retinal chromophore attached to the side chain of Lys-216 via a protonated Schiff base. The retinal is located about halfway through the membrane and sustains an angle of $\approx$70° with the membrane normal. Trimers of bR form two-dimensional crystalline patches in the plasma membrane. These purple membrane fragments (pm) can be isolated as sheets of about 0.5-μm diameter. The structure of the bR molecule is known to $\approx$3-Å resolution from electron crystallography (4, 5), and thanks to recent successes in preparing three-dimensional crystals of bR, to 2.3-Å resolution from x-ray crystallography (6, 7). The protein is the paradigm of the larger family of seven-helix receptors found throughout the living world from Archaea to mammals.

Light absorption by retinal initiates a chain of reactions called the photocycle. This photocycle is usually represented as a sequence of spectroscopically characterized intermediates (8): bR—K—L—M—N—O—bR.

In the excited state the retinal undergoes a cis/trans isomerization around the C=C(13,14) double bond, which is completed in the bR–K transition. The primary form of energy storage is presumably charge separation and/or mechanical strain caused by conformational changes. This energy is converted in several thermally activated steps through the subsequent metastable intermediate states, and a proton is transported while the system returns to the initial state. Understanding the mechanism will require a detailed description of the molecular events occurring during the cycle.

Photoelectric methods are widely used to follow the charge motions in ion pumps. Light-induced currents carry information about the transported charge and the protein conformational changes accompanying the function. Various experimental techniques have been developed to measure the charge movement with high time resolution. One major family of techniques involves incorporation of pm in an oriented fashion into liposomes (9) or attaching them to planar bimolecular lipid membranes (10, 11) that separate two aqueous compartments. A different approach uses pm suspension, where the permanent electric dipole moment, parallel to the membrane normal, orients the pm in a dc electric field of moderate strength (12). If a suspension of oriented pm is excited by a laser flash, the intramolecular charge displacement can be measured as a displacement current by electrodes immersed in the electrolyte (13). When the orientation is "frozen" in a gel, the system remains stable and, in contrast to suspensions, it enables long, repetitive data acquisition in the absence of an external orienting electric field (14). Because the sample is well defined and a quantitative analysis of the photoelectric signal is possible, one can determine the charge displacements during each step of the photocycle (15). This technique has the important advantage that spectroscopic changes can be recorded on the same sample.

Fundamental for all photoelectric methods is asymmetry of the studied object. Bacteriorhodopsin must be oriented in both the membrane and suspension methods to measure a net current flow macroscopically. However, in all model systems, bR is oriented only in the direction of the membrane normal. Around this axis the bR molecules are arranged rotationally randomly. Because of this cylindrical symmetry, only one spatial component of the charge displacement parallel to the

The publication costs of this article were defrayed in part by page charge payment. This article must therefore be hereby marked "*advertisement*" in accordance with 18 U.S.C. §1734 solely to indicate this fact.

PNAS is available online at www.pnas.org.

Abbreviations: bR, bacteriorhodopsin; pm, purple membrane fragments.

‡To whom reprint requests should be addressed. e-mail: derandra@everx.szbk.u-szeged.hu.

membrane normal can be followed: all other components cancel. For the full description of the charge displacement it is, however, necessary to determine all three spatial components of the photocurrent, and this requires nearly perfect orientation, which can be achieved by the combination of electric and magnetic fields (16). We have recently shown that it is feasible to measure the lateral components of the photocurrent (17) if the cylindrical symmetry of the system is broken by photoselection. The sample of oriented pm is excited by low-intensity light of appropriate linear polarization so that bR molecules oriented in one direction, are preferentially excited, and the in-plane component of the photocurrent, which contains information about the lateral charge motion, can be recorded.

Here we describe a further elaboration of the method, which determines the three spatial components of the charge displacement quantitatively and correlates the charge displacements to absorption kinetics of the photocycle. The results are discussed and related to predictions from molecular dynamics calculations (18–20).

MATERIALS AND METHODS

Sample Preparation. The experiments described here require a suspension of pm with nearly perfect orientation, which cannot be achieved with a dc electric field alone, because in a high electric field two effects counteract orientation: (*i*) perturbation by an induced dipole moment, perpendicular to the permanent dipole moment and (*ii*) migration and a resulting shear of the membrane fragments because of the net electric charge of pm (12, 21). A high magnetic field will align the membranes perfectly, but because the alignment is caused by an induced magnetic dipole, it cannot orient them facing in the same direction. Therefore, orientation by the combination of electric and magnetic fields was introduced (16). Here the initial orientation, achieved by short exposure to a moderate dc electric field, is improved by the subsequent application of a magnetic field while the oriented membranes are being immobilized in the polymerizing gel. The procedure aligns the membrane sheets with their permanent dipoles parallel to the field, pointing in the same direction, and is not impaired by the disturbing effects present during the application of a strong electric field.

Pm fragments prepared by the standard procedure (1) were oriented and immobilized in gel as follows (16). Suspensions containing 50 μM pm, 15% acrilamide, 0.8% *N*,*N*′-methylenebisacrilamide, 1% tetramethylethylenediamine (TEMED), and 0.3% ammonium persulfate were filled into cuvettes of 20 × 15 × 10 mm fitted with platinized Pt electrodes. An electric field of 20 V/cm was first applied to orient the pm, and the sample was then positioned in a 17.5-T magnetic field (Max Planck Institute High Magnetic Field Laboratory, Grenoble, France). Samples were also prepared with magnetic ordering only. In this case the pm are aligned rather than oriented, i.e., the membrane sheets are parallel, but their sidedness (overall pumping direction) is random. Alignment of the membranes in the suspension and gel was checked by magnetic birefringence measurements (22) and were found to be close to perfect. Further technical details of the sample preparation can be found in ref. 16.

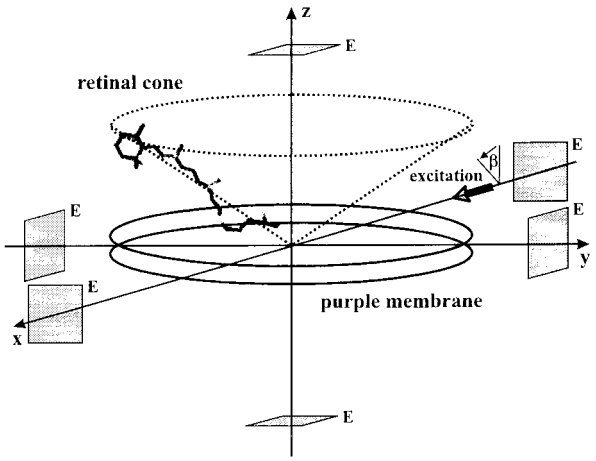

FIG. 1. Geometry of a pm oriented with its membrane normal coincident with the laboratory fixed *z* axis. The individual retinal chromophores' transition dipoles form a cone about this axis. The actinic laser pulse propagates along the laboratory fixed *x* axis with its polarization vector making an angle β with the *z* axis. The rectangular symbols represent the measuring electrodes (E).

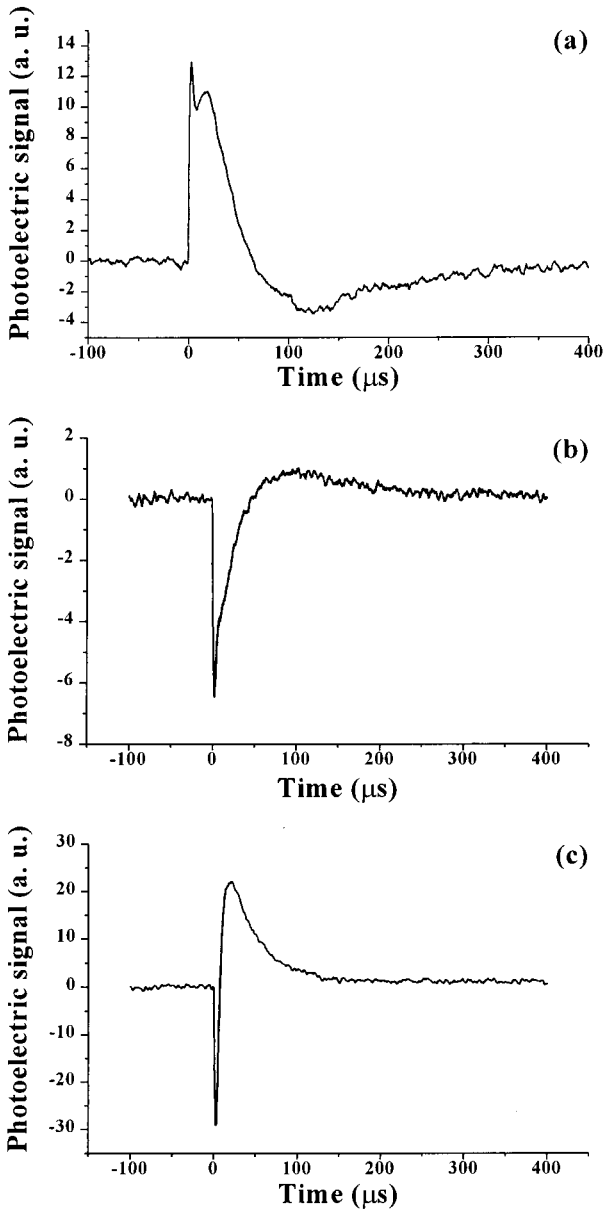

FIG. 2. Time-dependent photocurrents measured on pm oriented with the electric-magnetic field orientation method, in the three perpendicular laboratory fixed spatial directions. The signals were detected with electrode pairs oriented along the corresponding Cartesian axes. (*a*) $I_x(t)$. (*b*) $I_y(t)$. (*c*) $I_z(t)$.

Measuring Techniques. Cubes (1 × 1 × 1 cm) were cut out of gels with $OD_{575} = 2$ and were placed in a square measuring cell with three pairs of platinized Pt electrodes aligned along the *x*, *y*, and *z* axes (Fig. 1). Distance between the electrodes

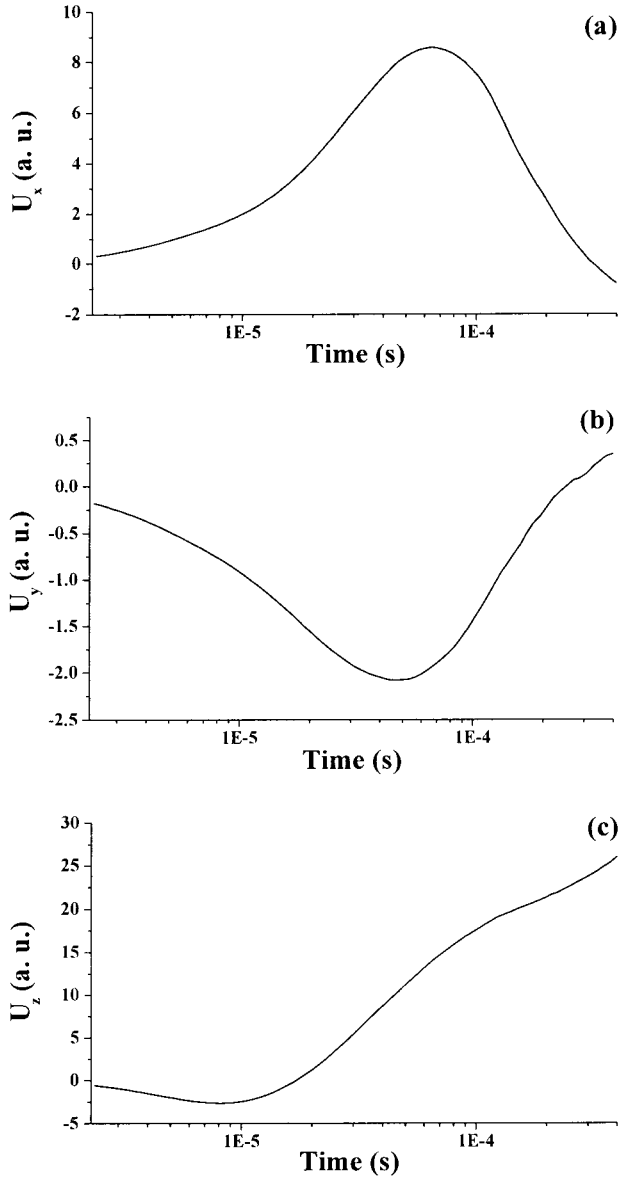

FIG. 3. Integral of the photoelectric signals in Fig. 2. $U_x(t)$ (*a*), $U_y(t)$ (*b*), and $U_z(t)$ (*c*) are linearly dependent on the net electric dipole moment of the photocycle intermediates (see text).

was 2 cm. Special care was taken to shield the electrodes from the exciting light to avoid artifacts caused by light scattering.

Fig. 1 shows the geometry of optical properties of a purple membrane oriented with its permanent dipole moment along the *z* direction. Samples were excited by polarized, 10-ns laser flashes of 100-μJ energy, from an excimer- laser-pumped dye laser (Rhodamine 6G), propagating in the *x* direction. The plane of polarization sustained angel $\beta = 45^o$ with the *z* axis. The signals were detected with the electrode pairs, amplified by voltage amplifiers, and stored in a transient recorder (LeCroy 9310L).

Absorption kinetics were measured on the same samples used in the electric measurements, under the same conditions (pH 6, 23°C). Spectral changes following the laser excitation were detected at logarithmically equidistant time delays from 300 ns to 400 μs, in the 350–750 nm wavelength range, with a gated Optical Multichannel Analyser (Spectroscopy Instruments, Gilching, Germany). Singular value decomposition provided the effective rank of the data matrix consisting of the time-resolved difference spectra, and the matrix was reconstructed and the noise filtered by using the significant singular value decomposition components only. The absorption spectra of the intermediates were derived from the difference spectra by using the Monte Carlo search algorithm described earlier (23). The concentration changes of the intermediates were calculated from the nonnegative linear least-squares fit of the pure intermediate spectra to the difference spectra. These time-resolved concentration changes were fitted by a linear photocycle scheme with reversible reactions to obtain the final intermediate concentrations, $c_i(t)$, by using the RATE 2.1 program written by Géza Groma. Further mathematical analysis of the data was carried out with the MATLAB program package.

Principles of the Method. Excitation with linearly polarized light allows measuring the in-plane components of the electric signal by breaking the intrinsic rotational symmetry of the sample around the *z* axis. We denote the three Cartesian component vectors of the directly detected electric signal by I_x, I_y and I_z, respectively.

Presuming perfect orientation and by using plausible assumptions (17, 24), the following matrix formula can be derived.

$$I_k(t) \propto \sum_j f_{jk} \sum_i \mu_i^j \frac{d}{dt} c_i(t) \qquad [1]$$

where j,k = *x*, *y*, or *z*, c_i is the concentration of the *i*th intermediate state, and the f_{jk} matrix element gives the weight of the μ_i^j dipole component relative to the *k* direction in the laboratory fixed-coordinate system. Note that the undefined proportionality constant in Eq. **1** depends on the ionic relaxation around the pm (15). Because of the membrane anisotropy and other reasons discussed in ref. 17, it must be different in the different Cartesian directions. By using the assignments of Fig. 1, f_{jk} can be written in a diagonal form:

$$[f_{jk}] = \begin{bmatrix} -\sin\beta\cos\beta & 0 & 0 \\ 0 & -\sin\beta\cos\beta & 0 \\ 0 & 0 & f_{zz}(\beta) \end{bmatrix} \qquad [2]$$

i.e., μ_i^j's are separated in this case in such a way that they contribute only to the corresponding $I_j(t)$'s. It is also easily seen from Eq. **2** that $I_x(t)$ and $I_y(t)$ have their maxima at $\beta = \pm 45^o$. The analytical form of $f_{zz}(\beta)$ has also been obtained. It (and, consequently I_z) has a minimum at $\beta = 0°$ and a maximum at $\beta = 90°$.

If the orientation is not perfect, $[f_{jk}]$ cannot be written in a diagonal form, that is, the measured $I_y(t)$ will be "contaminated" by μ_i^z's, as already discussed in ref. 16. By using symmetry arguments, it was also pointed out there that, in case of a magnetically aligned sample, only the μ_i^x components contribute to the measured signal.

To determine the corresponding μ_i^j values, the linear combination of $c_i(t)$'s was fitted to the time integral functions of $I_k(t)$'s ($U_k(t) = \int_0^t I_k(t)dt$).

RESULTS

Fig. 2 *a–c* show traces detected in different spatial dimensions, $I_x(t)$, $I_y(t)$, and $I_z(t)$, representing the Cartesian components of the photoelectric current measured on a sample containing pm oriented with the combination of electric and magnetic fields. As we pointed out earlier (ref. 24; *Materials and Methods*), the time-integral function of the photocurrent is proportional to the potential difference generated by the charge displacements during the pumping process, and it is properly scaled in terms of the dipole moment changes accompanying the photocycle of bR. Therefore, the integrated curves, $U_x(t)$, $U_y(t)$ and $U_z(t)$ were considered in the subsequent analysis (Fig. 3). Fig. 4

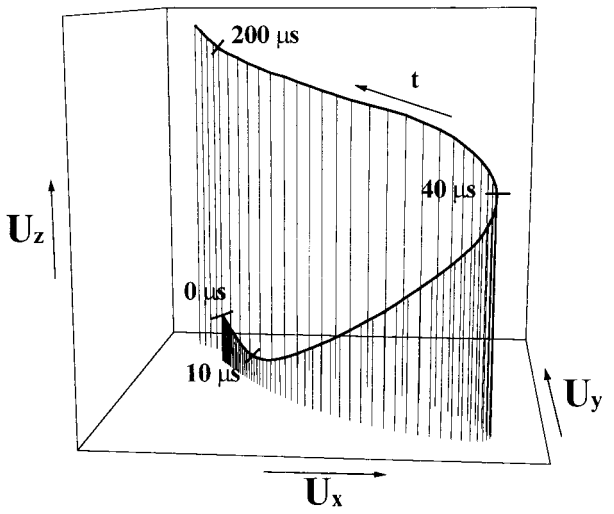

FIG. 4. Three-dimensional representation of the resultant integrated photocurrent, D(t), whose Cartesian components, $U_x(t)$, $U_y(t)$, and $U_z(t)$ are depicted in Fig. 3.

shows a three-dimensional trajectory defined by the resulting dipole moment vector $D(t) = [U_x(t),U_y(t),U_z(t)]$ in the first 400 μs of the photocycle.

From the definition of the electric dipole moment, it follows that this trajectory also characterizes the motion of the electric charge center of bR molecules during the photocycle. For a single molecule, however, we assume a discrete stationary value for the dipole moment of an intermediate (denoted by μ_i, where *i* stands for the actual photocycle intermediate). The measured D(t) is a smooth function related to the whole sample, which always contains a mixture of intermediates. The corresponding μ_i's, therefore, can be determined, if we know the time course of the concentration of the photocycle intermediates $[c_i(t)]$ in the macroscopic sample (see *Materials and Methods*). To determine the latter, absorption kinetics were measured on the same sample, under the same conditions, in addition to the photoelectric experiments. Difference spectra detected at various time delays after the exciting flash are shown in Fig. 5. A rank of 3 for the data matrix constructed from the time-resolved difference spectra was obtained by singular value decomposition. This establishes that three spectrally distinct intermediates, K, L, and M, are present in the time window of the measurement (300 ns–400 μs), i.e., no

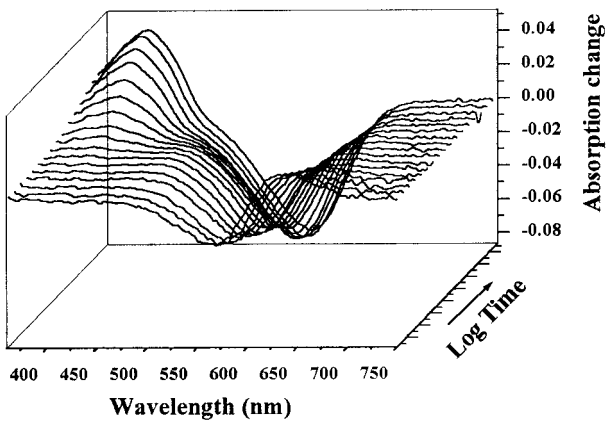

FIG. 5. Difference spectra in the visible wavelength range measured at logarithmically equidistant time delays after the laser flash excitation of electric–magnetic field orientation method-oriented pm. The evolution of the spectra is characteristic of the early transformation of the K intermediate to L and the subsequent accumulation of the blue-absorbing M intermediate.

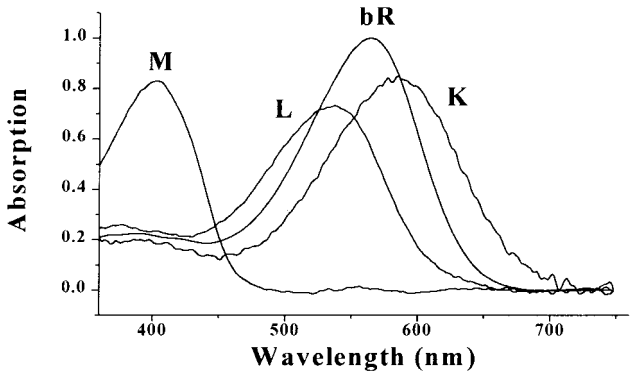

FIG. 6. Calculated absorption spectra of the photocycle intermediates K, L, and M, as well as that of the initial bR form. Spectra were obtained from the difference spectra in Fig. 5 with the Monte Carlo-based search algorithm. Substates of L and M are spectrally indistinguishable.

indication for the subsequent intermediates N and O was found. The absorption spectra of the K, L, and M intermediates (Fig. 6), as well as the corresponding time dependent concentrations (Fig. 7), were determined according to ref. 23, and the widely considered and tested photocycle model bR $\Rightarrow$ K $\rightleftharpoons$ L_1 $\rightleftharpoons$ L_2 $\rightleftharpoons$ M_1 $\rightleftharpoons$ M_2 was used to calculate the intermediate concentrations up to 400 μs.

The result of a multilinear regression fit of D(t) with linear combinations of $c_i(t)$'s yielded the μ_i values shown in Fig. 8. As for the interpretation of the results in the molecular coordinate system, a positive μ_i^z corresponds to the displacement of a positive charge in the direction of the overall proton pumping. A positive μ_i^y results from the displacement of a positive charge parallel to the projection of the retinal transition dipole moment onto the membrane plane, roughly from helix E toward helix A. Finally, a positive μ_i^x corresponds to the displacement of a positive charge perpendicularly to both μ_i^y and μ_i^z, approximately from the direction of helix C to helix F.

The μ_i's determined in this way may contain errors from several sources. First, the correct photocycle model cannot be uniquely determined in most cases unless certain assumptions are made, such as: first-order kinetics for the elementary reactions (25), plausible restrictions for the calculated absorption spectra of the intermediates (23, 26) and the photocyle scheme (24, 27), etc. Another problem arises when the criterion of linear independency for the set of $c_i(t)$'s is poorly satisfied. In addition to the measuring errors, these

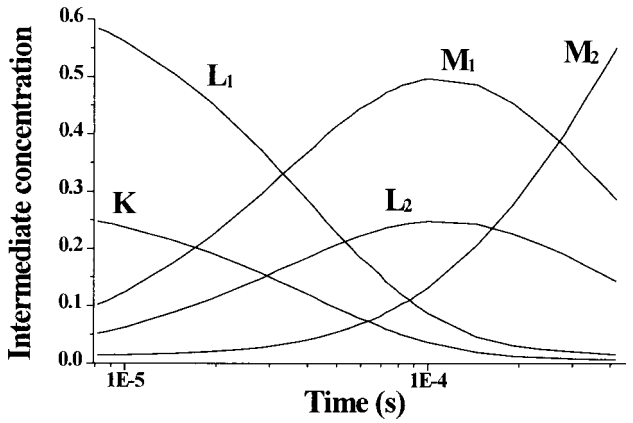

FIG. 7. Intermediate kinetics obtained after fitting the linear, reversible photocycle scheme (see text) to the intermediate concentrations calculated by the nonnegative least-squares fit of the pure intermediate spectra to the time-dependent difference spectra.

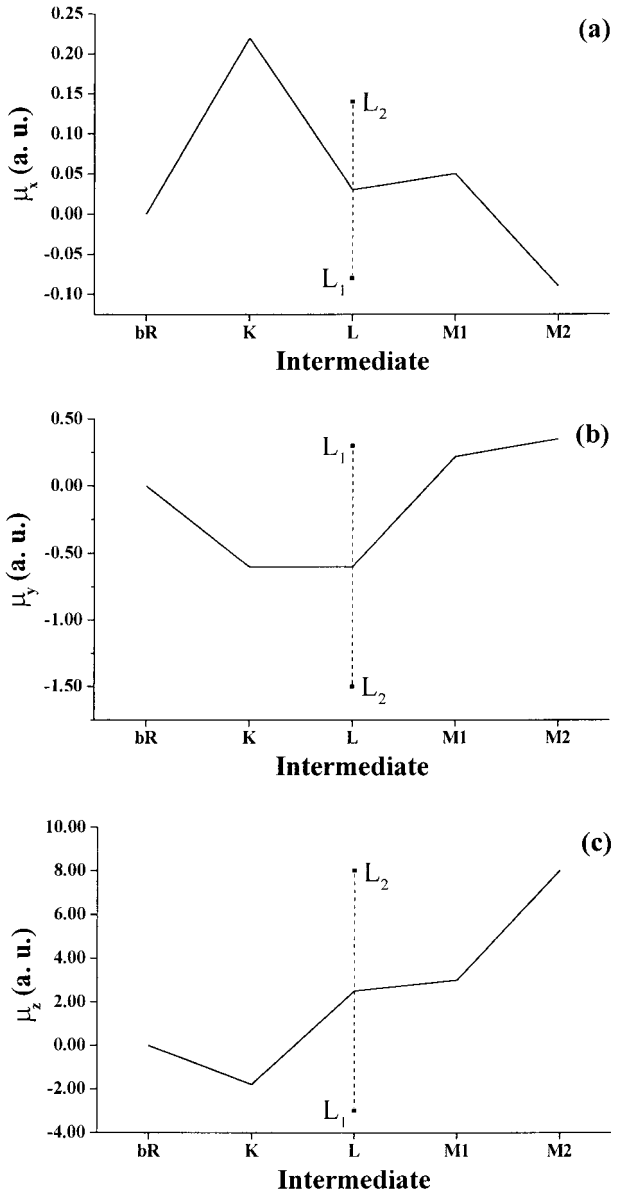

FIG. 8. Dipole moment changes of the photocycle intermediates relative to the initial state obtained from the three-dimensional photoelectric measurements. The individual dipole moments for the two L substates provided by our analysis were averaged to yield a single value comparable to the corresponding value from molecular dynamics calculations.

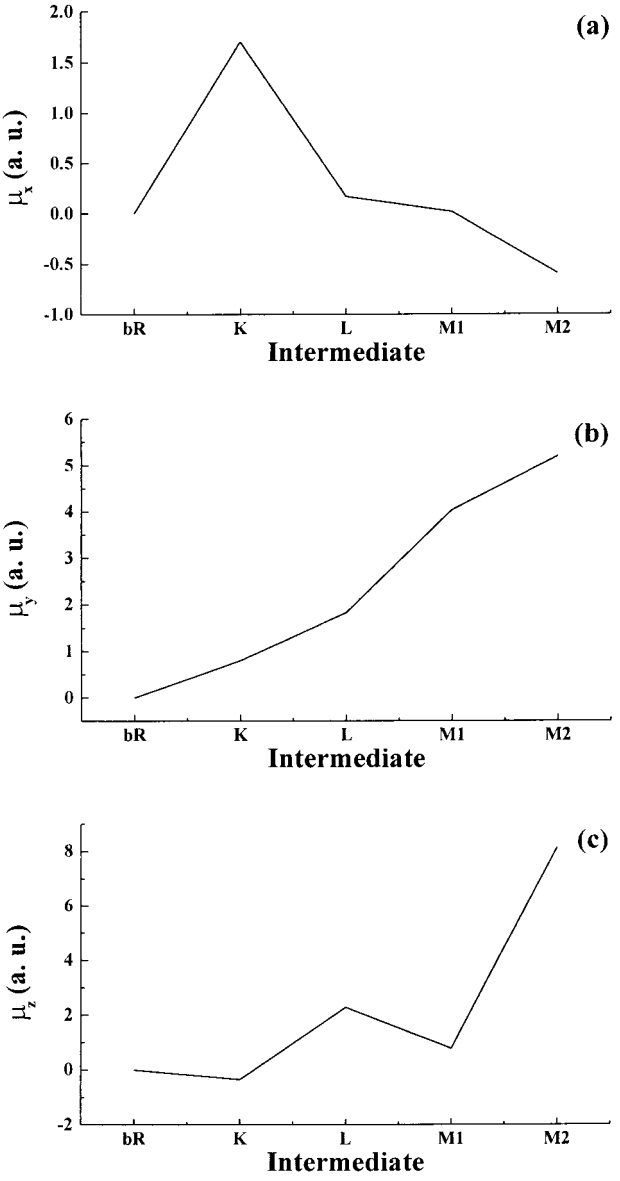

FIG. 9. Dipole moment changes of the photocycle intermediates relative to the initial state computed from the atomic coordinates and partial charges provided by molecular dynamics calculations (refs. 17 and 18; K. Schulten, personal communication).

are the major sources contributing to the uncertainty of the μ_i values.

In the simplest photocyle model that could account for the absorption kinetic changes in the time window of the measurements (i.e., the "first half of the photocycle"), a second L-like intermediate (L_2) in a rapid equilibrium with M_1 had to be assumed. The model with a single L yielded a considerably poorer fit, similar to some earlier observations (24, 26, 29). As a consequence of the rapid equilibrium, the time courses of L_2 and M_1 are nearly identical, which is reflected in high and mutually dependent error levels of the corresponding calculated dipole moments. Nevertheless, the results are consistent with earlier experimental data, obtained under different circumstances (13, 28), as well as with molecular dynamics calculations for the early events (up to the K intermediate) of the photocycle (18).

Table 1. Calculated electric dipole moment changes of the photocycle intermediates relative to bR

	μ_K			μ_L			μ_{M1}			μ_{M2}		
Group	*x*	*y*	*z*	*x*	*y*	*z*	*x*	*y*	*z*	*x*	*y*	*z*
1	1.70	0.80	−0.35	0.17	1.83	2.27	0.02	4.03	0.78	−0.59	5.19	8.13
2	—	—	—	5.07	5.28	0.10	1.41	7.85	−0.27	3.69	4.00	6.59
				0.56	14.0	11.5						

Data taken from the molecular dynamics structures provided by Schulten (Group 1) and Scharnagl *et al.* (Group 2). Data from Group 2 involved no K intermediate but two L intermediates.

DISCUSSION

As indicated in *Materials and Methods*, the experimentally determined μ_i^k values contain an undefined proportionality constant that is different in the three spatial directions. Consequently, the Cartesian components of a μ_i vector cannot be directly compared. However, the related μ_i^x, μ_i^y, and μ_i^z components do contain important information about charge rearrangements inside the protein during the photocycle; therefore, their comparison with theoretically predicted data is of primary interest.

The later part of the photocycle still lies beyond the time window of traditional molecular dynamics theory. Based on the high-resolution structure of bR determined by diffraction experiments, several attempts have been made by using semiempirical or classical force field calculations and the method of simulated annealing to compute the further progression of the photocycle (18–20, 30). Taking into account some known empirical parameters (p*K*'s, Fourier-transformed IR data, etc.) and by using plausible assumptions, structures for the L and M intermediates have also been published. We have calculated the μ_i values from two corresponding structures by using the atomic coordinates and partial charge values, which include the surrounding water molecules in addition to the atoms of bR (C. Scharnagl and K. Schulten, personal communication). Different molecular dynamics calculations yielded slightly different intermediate structures. Comparing the dipole moments (Table 1), one can conclude that the μ_i parameters represent a sensitive measure of these structural differences. The publications of Schulten's group (18, 19) contain a more complete data set, including the K intermediate, even though they considered only one L intermediate in the photocycle. To make our results directly comparable with their data, a single value (μ_L) stands for the experimentally determined dipole moment of the L intemediates in Fig. 8, representing the arithmetic average of μ_{L1} and μ_{L2}. Considering the numerous factors that may contribute to uncertainties of both the experimental and the theoretical values related to charge motions in the *x–z* plane, we find a noteworthy correlation between the normalized μ_i values determined by the two entirely different methods (Figs. 8 and 9).

Preliminary analysis regarding the assignment of components of the electric signal to rearrangements of particular charged and dipolar groups inside the bacteriorhodopsin molecule suggests that, while proton motion makes a major contribution to the signals measured in the *z* direction, the signals measured in the *x* and *y* directions are apparently dominated by the reorientation and redistribution of water molecules (unpublished data).

These results imply that there is a good chance to find an improved theoretical model that could account for all of the experimental results (including the observed charge displacements in the *y* direction), for which our method will provide the decisive test. Establishing such a model for the functional description of an ion pump protein at atomic level should have a strong impact on protein research in general.

The authors thank Profs. Klaus Schulten and Christina Scharnagl for sending us the results of their molecular dynamics calculations. We also thank Dr. G. Rikken for his technical help during sample preparation in the Grenoble High Magnetic Field Laboratory and Dr. G. Groma for providing the program (RATE 2.1) used in the fitting of kinetic models. This work was supported by grants from the Hungarian Scientific Research Fund (OTKA T29814, OTKA T017017, and OTKA T020470) and by a North Atlantic Treaty Organization Collaborative Research Grant (CRG 930419).

1. Oesterhelt, D. & Stoeckenius, W. (1974) *Methods Enzymol.* **31,** 667-678.
2. Lanyi, J. K. (1993) *Biochim. Biophys. Acta* **1183,** 241–261.
3. Ebrey, T. G. (1993) in *Thermodynamics of Membranes, Receptors and Channels*, ed. Jackson, M. (CRC, Boca Raton, FL), pp. 353–387.
4. Kimura, Y., Vassylyev, D. G., Miyazawa, A., Kidera, A., Matsushima, M., Mitsuoka, K., Murata, K., Hirai, T. & Fujuyoshi, Y. (1997) *Nature (London)* **389,** 206–210.
5. Grigorieff, N., Ceska, T. A., Downing, K. H., Baldwin, J. M. & Henderson, R. (1996) *J. Mol. Biol.* **259,** 393–421.
6. Pebay-Peyroula, E., Rummel, G., Rosenbusch, J. P. & Landau, E. M. (1997) *Science* **277,** 1676–1681.
7. Luecke, H., Richter, H. T. & Lanyi, J. K. (1998) *Science* **280,** 1934–1937.
8. Lozier, R. H., Bogomolni, R. A. & Stoeckenius, W. (1975) *Biophys. J.* **15,** 955–962.
9. Skulachev, V. P. (1979) *Methods Enzymol.* **55,** 586–603.
10. Dancsházy, Z. & Karvaly, B. (1976) *FEBS Lett.* **72,** 136–138.
11. Bamberg, E., Dencher, N. A., Fahr, A. & Heyn, M. P. (1981) *Proc. Natl. Acad. Sci. USA* **78,** 7502–7506.
12. Keszthelyi, L. (1980) *Biochim. Biophys. Acta* **598,** 429–436.
13. Keszthelyi, L. & Ormos, P. (1980) *FEBS Lett.* **109,** 189–194.
14. Dér, A., Hargittai, P. & Simon, J. (1985) *J. Biochem. Biophys. Methods* **10,** 295–300.
15. Keszthelyi, L. & Ormos, P. (1989) *J. Membr. Biol.* **109,** 193–200.
16. Dér, A., Tóth-Boconádi, R., Keszthelyi, L., Kramer, H. & Stoeckenius, W. (1995) *FEBS Lett.* **377,** 419–420.
17. Dér, A. & Ormos, P. (1995) *Biophys. Chem.* **56,** 159–163.
18. Humphrey, W., Xu, D., Sheves, M. & Schulten, K. (1995) *J. Phys. Chem.* **99,** 14549–14560.
19. Xu, D., Sheves, M. & Schulten, K. (1995) *Biophys. J.* **69,** 2745–2760.
20. Scharnagl, C., Hettenkofer, J. & Fischer, S. F. (1994) *Int. J. Quantum Chem.* **21,** 33–56.
21. Barabás, K., Dér, A., Dancsházy, Z., Marden, M., Ormos, P. & Keszthelyi, L. (1983) *Biophys. J.* **43,** 5–11.
22. Maret, G. & Weill, G. (1983) *Biopolymers* **22,** 2727–2744.
23. Gergely, C., Zimányi, L. & Váró, G. (1997) *J. Phys. Chem.* **101,** 9390–9395.
24. Dér, A., Tóth-Boconádi, R. & Száraz, S. (1992) *Colloq. INSERM* **221,** 197–200.
25. Nagle, J. F. (1991) *Biophys. J.* **54,** 476–487.
26. Zimányi, L. & Lanyi, J. K. (1993) *Biophys. J.* **64,** 240–251.
27. Ludmann, K., Gergely, C. & Váró, G. (1998) *Biophys. J.*, in press.
28. Ludmann, K., Gergely, C., Dér, A. & Váró, G. (1998) *Biophys. J.*, in press.
29. Gergely, C., Ganea, C., Groma, G. & Váró, G. (1993) *Biophys. J.* **65,** 2478–2483.
30. Engels, M., Gerwert, K. & Bashford, D. (1995) *Biophys. Chem.* **56,** 95–104.